# Topographical cues regulate the crosstalk between MSCs and macrophages

CrossMark

Gema Vallés [a, b], Fátima Bensiamar [a, b], Lara Crespo [a, b], Manuel Arruebo [b, c], Nuria Vilaboa [a, b], Laura Saldaña [a, b, *]

[a] Hospital Universitario La Paz-IdiPAZ, Paseo de la Castellana 261, 28046 Madrid, Spain
[b] Centro de Investigación Biomédica en Red de Bioingeniería, Biomateriales y Nanomedicina, CIBER-BBN, Spain
[c] Departamento de Ingeniería Química, Instituto de Nanociencia de Aragón (INA), Edificio I+D, Universidad de Zaragoza, C/Mariano Esquillor, 50018 Zaragoza, Spain

## ARTICLE INFO

## ABSTRACT

Implantation of scaffolds may elicit a host foreign body response triggered by monocyte/macrophage lineage cells. Growing evidence suggests that topographical cues of scaffolds play an important role in MSC functionality. In this work, we examined whether surface topographical features can regulate paracrine interactions that MSCs establish with macrophages. Three-dimensional (3D) topography sensing drives MSCs into a spatial arrangement that stimulates the production of the anti-inflammatory proteins $PGE_2$ and TSG-6. Compared to two-dimensional (2D) settings, 3D arrangement of MSCs co-cultured with macrophages leads to an important decrease in the secretion of soluble factors related with inflammation and chemotaxis including IL-6 and MCP-1. Attenuation of MCP-1 secretion in 3D co-cultures correlates with a decrease in the accumulation of its mRNA levels in MSCs and macrophages. Using neutralizing antibodies, we identified that the interplay between $PGE_2$, IL-6, TSG-6 and MCP-1 in the co-cultures is strongly influenced by the micro-architecture that supports MSCs. Local inflammatory milieu provided by 3D-arranged MSCs in co-cultures induces a decrease in monocyte migration as compared to monolayer cells. This effect is partially mediated by reduced levels of IL-6 and MCP-1, proteins that up-regulate each other's secretion. Our findings highlight the importance of topographical cues in the soluble factor-guided communication between MSCs and macrophages.

© 2014 The Authors. Published by Elsevier Ltd. This is an open access article under the CC BY-NC-ND license (http://creativecommons.org/licenses/by-nc-nd/3.0/).

## 1. Introduction

Regenerative medicine strategies using mesenchymal stem cells (MSCs) are expected to be a promising alternative approach to organ transplantation and tissue repair. Most tissue-engineering approaches involve culturing MSCs on three-dimensional (3D) scaffolds, which provide temporary support structures that recreate the natural shape of living tissues [1]. Implantation of scaffolds may elicit a host foreign body reaction that can interfere with its biological performance, impairing wound healing and tissue remodeling [2,3]. This inflammatory response is characterized by the presence of monocytes, macrophages and giant cells at the tissue–material interface [4,5]. In addition to the resident macrophages already present at the wound site, macrophage precursors are recruited from the blood. Macrophage infiltration into the injury site is highly regulated by gradients of different chemotactic factors including pro-inflammatory cytokines such as interleukin-6 (IL-6) and chemokines such as monocyte chemotactic protein-1 (MCP-1), macrophage inflammatory protein-1α (MIP-1α) and regulated upon activation normal T cell expressed and presumably secreted (RANTES) [6,7]. Activated macrophages secrete an array of inflammatory mediators into the tissue microenvironment that directs foreign body reaction and modulates wound healing [8].

Although MSCs exhibit prominent multi-lineage differentiation potential, current evidence indicates that the production of multiple paracrine factors underlies their regenerative mechanism [9]. MSCs secrete a broad spectrum of soluble factors that can alter the local milieu by contributing to angiogenesis, tissue repair, cytoprotection, native cell growth and alleviation of inflammation [10,11]. Paracrine mechanisms of MSCs include the modulation of

the inflammatory response mediated by monocyte/macrophage lineage cells [12,13]. Chemokines, anti-inflammatory cytokines, growth factors and other bioactive molecules secreted by MSCs regulate functional characteristics of macrophages. *In vitro* studies have shown that co-culture with MSCs induces macrophages to turn into a regulatory phenotype characterized by the expression of reduced levels of tumor necrosis factor-α (TNF-α) and IL-12 and increased levels of IL-10 [14,15]. Mechanisms of MSC immunomodulation involve the production of soluble factors including prostaglandin $E_2$ (PGE$_2$) and TNF-stimulated gene 6 protein (TSG-6) [16].

*In vivo*, cells are surrounded by a 3D extracellular matrix (ECM), which provides cell support, mechanical integrity and biological signaling [17]. ECM of native tissues possesses a unique, intricate, and often fractal topography comprised of a heterogeneous mixture of fibers, pores and ridges ranging from submillimeter to the nanometer scale [18]. Cell culture substrates and scaffolds with bioinspired topographic features drive MSCs into spatial arrangements that regulate their morphology, stemness maintenance and fate [19–21]. However, whether topographical cues can modulate the immunomodulatory properties of MSCs has not been explored yet. In this work, we investigate the effect of the tridimensionality of the substrate on the paracrine interactions that MSCs establish with macrophages. To this aim, MSCs seeded in 3D scaffolds or 2D surfaces were co-cultured with macrophages using a transwell insert system and levels of soluble factors related with inflammation and chemotaxis were quantified.

## 2. Materials and methods

### 2.1. Materials

Highly porous (>90%) synthetic scaffolds made of cross-linked polystyrene (Alvetex®) were purchased from Reinnervate (Durham, UK). These scaffolds (referred to as 3D substrates) were developed using an emulsion template technique to control the size of the pores [22]. Polyester membrane cell culture inserts (Corning, Lowell, MA) were used as flat permeable supports (referred to as 2D substrates). For cell culture experiments, scaffolds were immersed in 70% ethanol for 5 min, carefully aspirated and washed with PBS, according to the manufacturer's instructions. 3D and 2D substrates were incubated with DMEM supplemented with 15% (v/v) heat-inactivated FBS, 500 UI/ml of penicillin and 0.1 mg/ml of streptomycin for 15 min before cell seeding.

### 2.2. Cell culture

Purified human bone marrow-derived MSCs (CD105+, CD29+, CD44+, CD14−, CD34− and CD45−) were purchased from Lonza (Basel, Switzerland) and expanded in a defined medium (Lonza) consisting of MSC basal medium and Single Quots growth supplements containing fetal bovine serum (FBS), L-glutamine and penicillin/streptomycin. All experiments were performed below seven cell passages. Experiments were repeated in duplicate using seven different batches of MSCs obtained from donors aged 18–28 years. Human acute monocytic leukemia THP-1 cells (ECACC, Salisbury, UK) were grown in RPMI-1640 medium supplemented with 10% (v/v) heat-inactivated FBS, 500 UI/ml of penicillin and 0.1 mg/ml of streptomycin. Cells were maintained at 37 °C in a humidified 5% CO$_2$ incubator and kept in continuous logarithmic growth by passage every 3 days. To induce macrophage differentiation, cells were treated with 100 ng/ml 12-O tetradecanoyl phorbol 13-acetate (TPA) (Sigma, Madrid, Spain) for 12 h, thoroughly washed with PBS and incubated in fresh medium for a further 24 h (modified from Vallés et al. [24]). According to this protocol, TPA-treated THP-1 cells (dTHP-1) differentiate into plastic-adherent macrophage-like cells and express high levels of CD11b and CD14 (data not shown).

### 2.3. dTHP-1/MSC co-culture

MSCs and dTHP-1 were co-cultured using a polyester membrane cell culture insert that allows humoral contact of both cell types in the absence of direct cell-to-cell contact. THP-1 cells were seeded into six-well plates at a density of $4 \times 10^5$ cells/well and treated with TPA, as described above. dTHP-1 adhered to the bottom of the wells were washed with PBS and supplemented with a mixture of 50% RPMI and 50% DMEM, containing 12.5% (v/v) heat-inactivated FBS. Parallel groups of $8 \times 10^4$ MSCs were seeded directly in the inserts (2D conditions) or in scaffolds placed into the inserts (3D conditions) and cultured for 24 h. Then, the cells were washed with PBS and the inserts harboring MSCs were placed into the wells containing dTHP-1. Appropriate volumes of medium were added to achieve a final volume of 3 ml. As

controls, only dTHP-1 or MSCs were cultured in wells or inserts, respectively. Co-cultures were incubated for a further 72 h. For time-course experiments, aliquots of culture medium were collected at the indicated time points. Cell viability remained greater than 90% under all experimental conditions (data not shown).

### 2.4. Scanning electron and confocal microscopy analysis

Topographical features of the culture substrates were examined by scanning electron microscopy (SEM) using an FEI Quanta 200 Environmental scanning electron microscope (Hillsboro, OR). For the analysis of pore size distribution in the substrates, 300 pores randomly selected from 3 representative SEM images were manually outlined. The areas of pores were measured using ImageJ v1.34 image analysis software (http://rsbweb.nih.gov/ij) and the corresponding equivalent circle diameter (ECD) was calculated. To examine the influence of surface features on cell morphology, $8 \times 10^4$ MSCs were cultured for 3 days in 2D or 3D substrates. Attached cells were washed with PBS and fixed in 2.5% glutaraldehyde for 30 min at room temperature. Samples were dehydrated in a graded ethanol series (from 30% to 100%, v/v) for 15 min at each step and critical point dried with CO$_2$ (Quorum Technologies CPD7501, Newhaven, UK). Once dried, the samples were examined by SEM in low-vacuum mode. Cell morphology was also examined after fixation of MSCs with a solution of 2.5% glutaraldehyde using a confocal microscope (Leica TCS SPE, Leica Microsystems, Heidelberg, Germany). The autofluorescent signal of the biological samples due to glutaraldehyde fixation was collected in the emission ranges 567–689 nm after excitation with laser line at 532 nm. The surface of 3D scaffolds was directly visualized by reflection under excitation with a laser wavelength of 488 nm and by collecting the emission in the range 480–500 nm, as previously described [23]. Since topographical features of transwell membranes were below the resolution limit of 200 nm in confocal microscopy, only 3D substrates were examined using this technique. Stacks of 1 μm optical sections spanning complete surfaces were captured and recorded. Image stacks of x–y optical sections acquired repeatedly in sequential steps along the z-axis were digitalized and processed for 3D reconstructions. Maximum projections and orthogonal projections were represented using the software developed by the microscope manufacturer (LEICA software LCS, version 2.5 Build 1227).

### 2.5. Inmunofluorescence assays

MSCs seeded in 2D or 3D substrates at a density of $8 \times 10^4$ cells/well were cultured for 3 days, fixed with 4% (w/v) formaldehyde in PBS and permeabilized with 0.1% Triton X-100 in PBS. For immunostaining, cells were blocked in PBS containing 2% bovine serum albumin (BSA) and 0.05% Tween 20 and then stained with a mouse anti-Sox-2 mAb and anti-STRO-1 mAb (both from Chemicon, Harrow, UK) diluted 1:50 in 1% BSA in PBS. After washing with 0.05% Tween in PBS, cells were incubated with Alexa-Fluor 488 secondary antibodies (Molecular Probes, Leiden, Holland) diluted 1:1000 (v/v) in PBS containing 1% BSA. After washing with 0.05% Tween in PBS, cells were examined using confocal microscopy.

### 2.6. ALP activity

MSCs seeded in 2D or 3D substrates at a density of $8 \times 10^4$ cells/well were cultured for 3 days in growth medium or 15 days in osteogenic induction medium (Lonza) consisting of MSC basal medium and the Single Quots© osteogenic supplements containing FBS, L-glutamine, penicillin/streptomycin, dexamethasone, ascorbate and β-glycerophosphate. To prevent nutrient exhaustion, osteogenic induction medium was partially replaced every 3 days with an equal volume of fresh medium. Alkaline phosphatase (ALP) activity was assayed in cell layers by determining the release of p-nitrophenol from p-nitrophenylphosphate (Sigma) at 37 °C and a pH of 10.5. The data were normalized to the total protein amounts in cell layers determined by the Bio-Rad protein assay (Bio-Rad Laboratories Inc., Hercules, CA), based on the Bradford dye-binding method, using BSA as standard.

### 2.7. Protein secretion

MSCs and dTHP-1 were co-cultured as described in Section 2.3. Culture media were collected, filtered and centrifuged at 1200 g for 10 min, supplemented with a mixture of protease inhibitors (17.5 mg/ml phenylmethylsulfonyl fluoride, 1 mg/ml pepstatin A, 2 mg/ml aprotinin, 50 mg/ml bacitracin, all from Sigma) and frozen at −80 °C. Human specific ELISA kits were used to measure MCP-1, RANTES and vascular endothelial growth factor (VEGF) (all from Ebioscience, Vienna, Austria), PGE$_2$ (Cayman Chemical Company, Ann Harbor, MI), macrophage colony-stimulating factor (M-CSF) (R&D Systems, Abingdon, UK), TSG-6 (Mybioscience, San Diego, CA) and the soluble form of the receptor activator of nuclear factor kappa-B ligand (RANKL) (Biomedica Gruppe, Vienna, Austria). The detection limits of the kits were 2.3 pg/ml for MCP-1, 4.2 pg/ml for RANTES, 7.9 pg/ml for VEGF, 15 pg/ml for PGE$_2$, 11.2 pg/ml for M-CSF, 39 pg/ml for TSG-6 and 1.5 pg/ml for RANKL. All procedures were performed following the manufacturer's instructions. The secreted TNF-α, IL-6, IL-10 and granulocyte macrophage colony-stimulating factor (GM-CSF) were detected using BD CBA Flex Sets (BD Biosciences, San Jose, CA) following the manufacturer's instructions. The data were acquired using a FACSCalibur flow cytometer and analyzed with the FCAP Array Software version 3.0 (BD Biosciences). The detection limits of the immunoassays were 3.7 pg/ml for TNF-α, 2.5 pg/ml for IL-6,

3.3 pg/ml for IL-10 and 0.2 pg/ml for GM-CSF. In some experiments, cell layers were washed exhaustively with PBS, extracted with $5 \times 10^{-2}$ M Tris–HCl pH 8.0, $5 \times 10^{-1}$ M NaCl and 1% Triton X-100 and supplemented with a mixture of protease inhibitors. RANTES levels in extracts were measured using the specific ELISA kit. The data were normalized to the total protein amounts.

### 2.8. Gene expression

MSCs and dTHP-1 were co-cultured as described in Section 2.3. Total RNA was prepared using TRI Reagent (Molecular Research Center, Inc., Cincinnati, OH, USA), following the manufacturer's instructions. Complementary DNAs were prepared from total RNA using AMV (Roche Applied Science, Indianapolis, IN) and random hexamers. Real-time quantitative PCR was performed using LightCycler FastStart DNA Master SYBR Green I and LightCycler detector (both from Roche Applied Science). Assays were conducted in duplicate. Quantitative expression values were extrapolated from standard curves, and normalized to β2-microglobulin (β2M). Specific oligonucleotide primers were: IL-6, 5′-CCCCAGGAGAAGATTCCAAA-3′ (forward primer, F), 5′-CCAGTGATGATTTTCACCAGG-3′ (reverse primer, R); cyclooxygenase-2 (COX-2), 5′-TGAGCATCTACGGTTTGCTG-3′ (F), 5′-

TGCTTGTCTGGAACAACTGC-3′ (R); TSG-6, 5′-TCACATTTCAGCCACTGCTC-3′ (F), 5′-AGACCGTGCTTCTCTGTGGT-3′ (R); MCP-1, 5′-CCCCAGTCACCTGCTGTTAT-3′ (F), 5′-TGGAATCCTGAACCCACTTC-3′ (R); RANTES, 5′-CGCTGTCATCCTCATTGCTA-3′ (F), 5′-GAGCACTTGCCACTGGTGTA-3′ (R); β2M, 5′-CCAGCAGAGAATGGAAAGTC-3′ (F), 5′-GATGCTGCTTACATGTCTCG-3′ (R).

### 2.9. Neutralizing antibody assays

MSCs and dTHP-1 were co-cultured for 24 h, washed twice with PBS and incubated for 48 h in 3 ml of serum-free medium either containing or not the corresponding neutralizing antibody. Neutralizing antibodies against PGE$_2$ (Cayman Chemical Company), TSG-6 (Santa Cruz, Heidelberg, Germany), IL-6 or MCP-1 (R&D Systems) were used at 1 μg/ml. Aliquots of culture medium were collected and levels of IL-6 and MCP-1 were quantified as described in Section 2.7.

### 2.10. Migration assays

Migration assays were conducted in 24-well plates carrying transwell inserts of 5 μm pore size (Corning). Briefly, THP-1 were washed twice, resuspended in serum-free RPMI at a density of $1.5 \times 10^6$ cells/ml and then loaded onto the inserts.
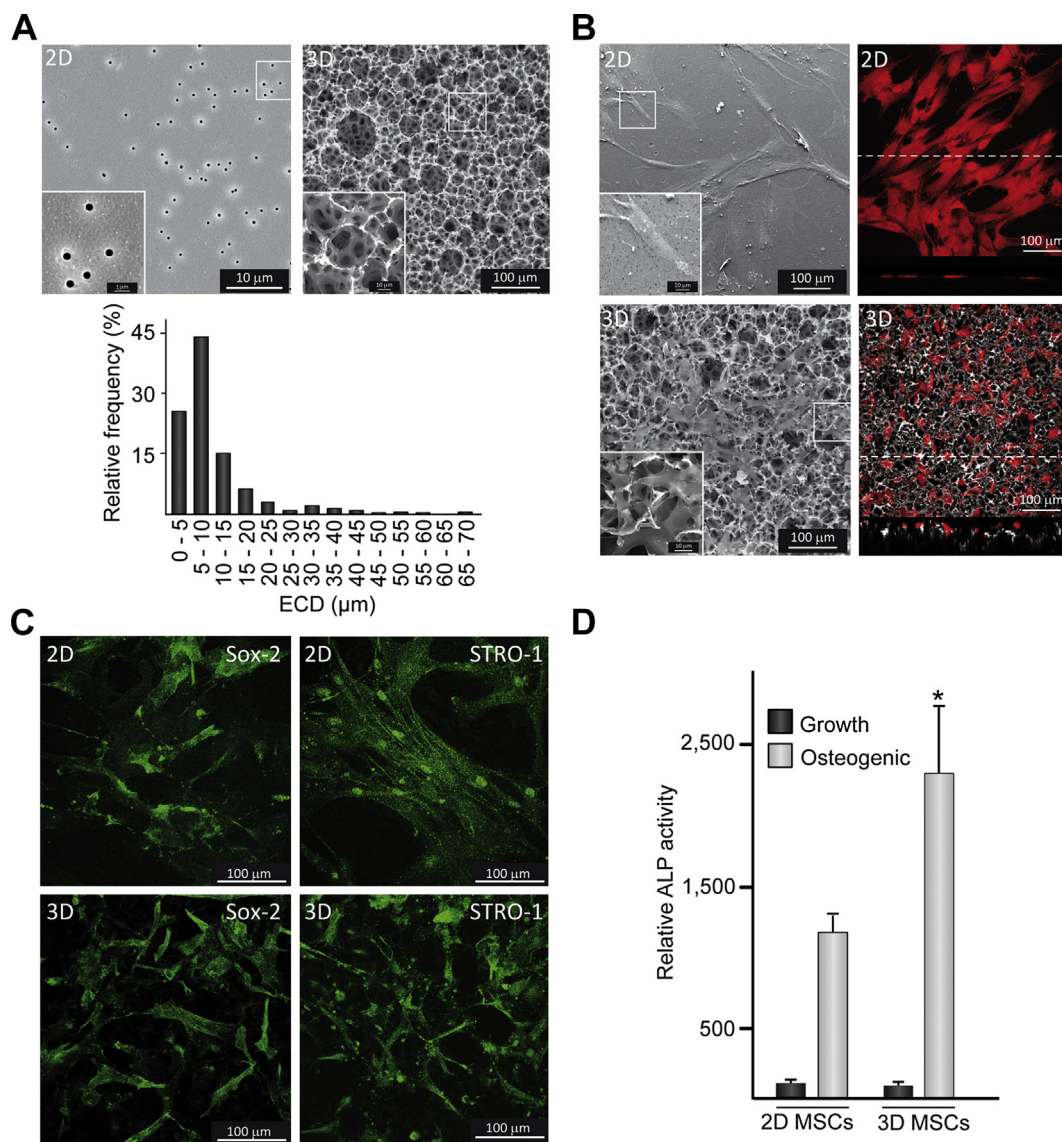


**Fig. 1.** MSC arrangement and phenotype in 2D or 3D substrates. (A) SEM images of 2D or 3D substrates and relative frequency histogram showing the equivalent circle diameter (ECD) of pores in 3D substrates. (B) Left panels: SEM images showing cell morphology in 2D or 3D substrates. Right panels: Confocal maximum projections of glutaraldehyde fixed cells (red) and the underlying surface detected by reflection. Confocal vertical (XZ) sections of the samples are shown at the bottom of the images. Dashed lines indicate the lines along which vertical sections were recorded. Insets in SEM images show higher magnification views of boxed areas. (C) Analysis of the undifferentiated stem cell markers Sox-2 and STRO-1 in MSCs cultured in 2D or 3D substrates. (D) ALP activity in MSCs seeded in 2D or 3D surfaces and cultured in growth or osteogenic medium. In these experiments, a relative activity value of 100 corresponded to about 1.5 ± 0.4 nmol/min.μg of total proteins. Each value represents the mean ± SD of five independent experiments. *$p < 0.05$ compared to 2D settings (For interpretation of the references to color in this figure legend, the reader is referred to the web version of this article.).

**Table 1**
Secretion of soluble factors from MSCs cultured in 2D or 3D substrates.

| | IL-6 | PGE$_2$ | TSG-6 | MCP-1 | VEGF | M-CSF | RANKL |
|---|---|---|---|---|---|---|---|
| 2D MSCs | 57.4 ± 14.9 | 6.0 ± 2.2 | 4.3 ± 1.6 | 27.8 ± 8.8 | 39.3 ± 10.7 | 3.8 ± 0.6 | 1.2 ± 0.1 |
| 3D MSCs | 34.1 ± 8.9* | 14.7 ± 6.1* | 9.8 ± 2.0* | 10.3 ± 2.9* | 27.0 ± 6.6 | 4.3 ± 1.3 | 0.6 ± 0.1* |

The data are expressed as pg/ml.µg of total proteins. Each value represents the mean ± SD of five independent experiments. *$p < 0.05$ compared to 2D MSCs.

**Table 2**
Time-dependent changes of TNF-α and IL-6 secretion in 2D co-cultures.

| | TNF-α | | IL-6 | |
|---|---|---|---|---|
| | dTHP-1 | dTHP-1/MSCs | MSCs | dTHP-1/MSCs |
| 24 h | 92.0 ± 15.6 | 78.2 ± 16.6 | 0.8 ± 0.2 | 10.7 ± 3.1$^{\&}$ |
| 48 h | 334.0 ± 32.2* | 225.4 ± 39.6*$^{,\&}$ | 1.2 ± 0.1* | 56.8 ± 16.0*$^{,\&}$ |
| 72 h | 377.2 ± 64.4* | 115.9 ± 23.0*$^{,\&}$ | 1.4 ± 0.3* | 77.7 ± 23.1*$^{,\&}$ |
| 96 h | 217.1 ± 27.6* | 54.3 ± 6.4$^{\&}$ | 1.4 ± 0.2* | 98.3 ± 22.3*$^{,\&}$ |

The data are expressed as pg of TNF-α and ng of IL-6 per ml of culture medium. Each value represents the mean ± SD of four independent experiments. *$p < 0.05$ compared to 24 h, $^{\&}p < 0.05$ compared to single-cultured cells.

Conditioned medium (CM) of co-cultures in 2D or 3D conditions, previously incubated in the absence or presence of 1 µg/ml human anti-IL-6 or anti-MCP-1 neutralizing antibody for 1 h at 37 °C, was placed in the bottom chamber. After 5 h of incubation at 37 °C with 5% CO$_2$, cells that migrated to the lower chamber were collected and counted employing the trypan blue dye exclusion method. Non-specific migration was assessed by using culture medium without serum.

### 2.11. Statistical analysis

The data are presented as means ± S.D. of several independent experiments. ANOVAs with Bonferroni's correction were used for post-hoc comparisons. All results were verified with corresponding non-parametric tests (Mann–Whitney $N$ pair $t$-test). The $p$-values <0.05 were considered statistically significant. All statistical analyses were performed using the Statistical Package for the Social Sciences, version 11.5 (SPSS Inc., Chicago, IL, USA).

## 3. Results

### 3.1. MSC morphology, phenotype and secretory profile in 2D or 3D substrates

SEM examination of 2D substrates revealed a flat surface with a homogeneous pore size distribution (0.51 ± 0.03 µm) (Fig. 1A). In contrast, 3D scaffolds displayed a rough surface morphology consisting of a microporous network with randomly oriented and interconnected pores. Frequency histogram of the EDC of pores in 3D substrates showed a heterogeneous size distribution ranging between 2 µm and 70 µm, with a higher percentage of small pores (90% with EDC ≤ 20 µm) (Fig. 1A). MSCs grown in transwells formed a 2D monolayer and exhibited a clearly expanded, typically elongated shape (Fig. 1B). Vertical sections obtained by confocal imaging showed MSCs cultured in 2D substrates from a lateral view and revealed that cells had a flat morphology. MSCs in 3D substrates displayed a smaller area and stellate morphology, with cytoplasmic extensions that penetrated into the pores. Compared to 2D substrates, orthogonal projections indicated that cells acquired a more rounded morphology on the rough and irregular surface of scaffolds. Analysis of cell growth for 1–3 days by the trypan blue dye exclusion method revealed a similar proliferation rate in MSCs cultured in 3D or 2D substrates (data not shown). MSCs were positively stained for the markers of undifferentiated cells Sox-2 and STRO-1 and no apparent differences were found between cells cultured in 2D or 3D surfaces (Fig. 1C). Positive staining of Sox-2 and STRO-1 was maintained in MSCs co-cultured with dTHP-1 (data not shown). To further confirm the retention of MSC phenotype, we quantified ALP activity, an early osteogenic marker, in cells cultured in 3D substrates. MSCs disposed in a 3D arrangement showed similarly low levels of ALP activity to those detected in 2D monolayer cells (Fig. 1D). ALP activity remained at baseline levels after co-culturing with dTHP-1 (data not shown). To assess whether MSCs cultured in the surfaces still maintained their differentiation capacity to the osteoblastic lineage, parallel sets of cells were cultured in osteogenic induction medium. Under these conditions, ALP activity greatly increased in both substrates and levels were higher in 3D than in 2D surfaces (Fig. 1D). Next, we evaluated the secretion of soluble factors from MSCs cultured in 3D or 2D substrates (Table 1). Compared to 2D samples, IL-6, MCP-1 and RANKL secretion was lower when MSCs were cultured in scaffolds while VEGF and M-CSF production was similar. Interestingly, cells disposed in a 3D arrangement secreted higher levels of PGE$_2$ and TSG-6 than 2D monolayer cells.

### 3.2. Establishment of an in vitro co-culture model

Next, we performed time-course experiments of TNF-α and IL-6 release from cultures of dTHP-1 and MSCs seeded in flat surfaces, respectively (Table 2). TNF-α secretion from dTHP-1 increased considerably from 24 to 48 h and sustained up to 72 h, after which a decrease occurred. Regarding IL-6 secretion from MSCs, production of this protein augmented after 48 h and this increase was maintained for the observation period of 96 h. The secretory profile of these inflammatory markers was modulated in co-cultures of both cell types. Exposure of dTHP-1 to MSCs for 48 h led to a significant attenuation in TNF-α levels, which further decreased for 72–96 h. IL-6 secretion greatly increased after co-culturing in a time-dependent manner. Since both maximum TNF-α release in dTHP-1 cultures and highest attenuation of this cytokine secretion by MSCs occur at 72 h, subsequent co-culture assays were carried out at this time point.

**Table 3**
TNF-α, IL-10, M-CSF, GM-CSF, VEGF and RANKL secretion in 2D or 3D co-cultures.

| | TNF-α | IL-10 | M-CSF | GM-CSF | VEGF | RANKL |
|---|---|---|---|---|---|---|
| dTHP-1 | 381 ± 138 | N.D. | 1400 ± 406 | N.D. | 6.1 ± 2.0 | N.D. |
| 2D MSCs | N.D. | N.D. | 124 ± 38 | N.D. | 1.4 ± 0.3 | 12 ± 5 |
| 3D MSCs | N.D. | N.D. | 109 ± 31 | N.D. | 0.7 ± 0.2 | 5 ± 1$^{\&}$ |
| dTHP-1/2D MSCs | 96 ± 25* | 106 ± 19* | 642 ± 62* | 4.4 ± 0.8 | 19.0 ± 2.8* | 10 ± 3 |
| dTHP-1/3D MSCs | 92 ± 29* | 102 ± 19* | 355 ± 91*$^{,\#}$ | 2.1 ± 0.4$^{\#}$ | 15.2 ± 3.9* | 5 ± 1$^{\#}$ |

The data are expressed as pg/ml of culture medium except for VEGF, which are expressed as ng/ml. Each value represents the mean ± SD of six independent experiments. $^{\&}p < 0.05$ compared to 2D MSCs, *$p < 0.05$ compared to single-cultured cells, $^{\#}p < 0.05$ compared to 2D co-cultures. N.D.: not detected.

### 3.3. Secretion of inflammatory cytokines and growth factors in 2D or 3D co-cultures

The effect of topographical cues on the production of specific factors involved in inflammation was evaluated in 2D or 3D co-cultures (Table 3). Co-culturing dTHP-1 with MSCs led to a decrease in TNF-α secretion and an increase in IL-10 levels, independently of the topographic features of the substrate. Quantification of *TNF-α* and *IL-10* mRNA transcripts in dTHP-1 revealed a pattern similar to the observed secretion profile (data not shown). Regarding hematopoietic growth factors, M-CSF secretion in co-cultures substantially increased as compared to MSCs but decreased with respect to dTHP-1. Protein levels were lower in 3D co-cultures as compared to the bidimensional model. Similar down-modulation in 3D co-cultures was observed for GM-CSF, which was not detected in single cultures. Secretion of the angiogenic factor VEGF was induced after co-culturing and levels were similar in both 2D and 3D settings. In contrast, 3D spatial arrangement of MSCs cultured in isolation or co-cultured with dTHP-1 induced a decrease in RANKL, a soluble factor involved in bone resorption. Secretion levels of this protein were not influenced by co-culturing with dTHP-1.

### 3.4. IL-6, PGE₂ and TSG-6 levels in 2D or 3D co-cultures

Co-culturing dTHP-1 with MSCs significantly increased the release of IL-6 and $PGE_2$ as compared to single cultures (Fig. 2A, B). TSG-6 levels in co-cultures were higher than those detected in MSCs but lower than those observed in dTHP-1 (Fig. 2C). Compared to 2D settings, IL-6 secretion decreased in 3D co-cultures while $PGE_2$ and TSG-6 production increased. Next, we studied the changes in gene expression of these cytokines, at the mRNA level, in dTHP-1, MSCs or in each cell type after co-culturing. MSCs grown in scaffolds expressed higher mRNA levels of *COX-2*, the key regulator of $PGE_2$ synthesis, and *TSG-6* than 2D monolayer cells (Fig. 2E, F). Compared to single-cultured cells, *IL-6*, *COX-2* and *TSG-6* mRNA levels in MSCs
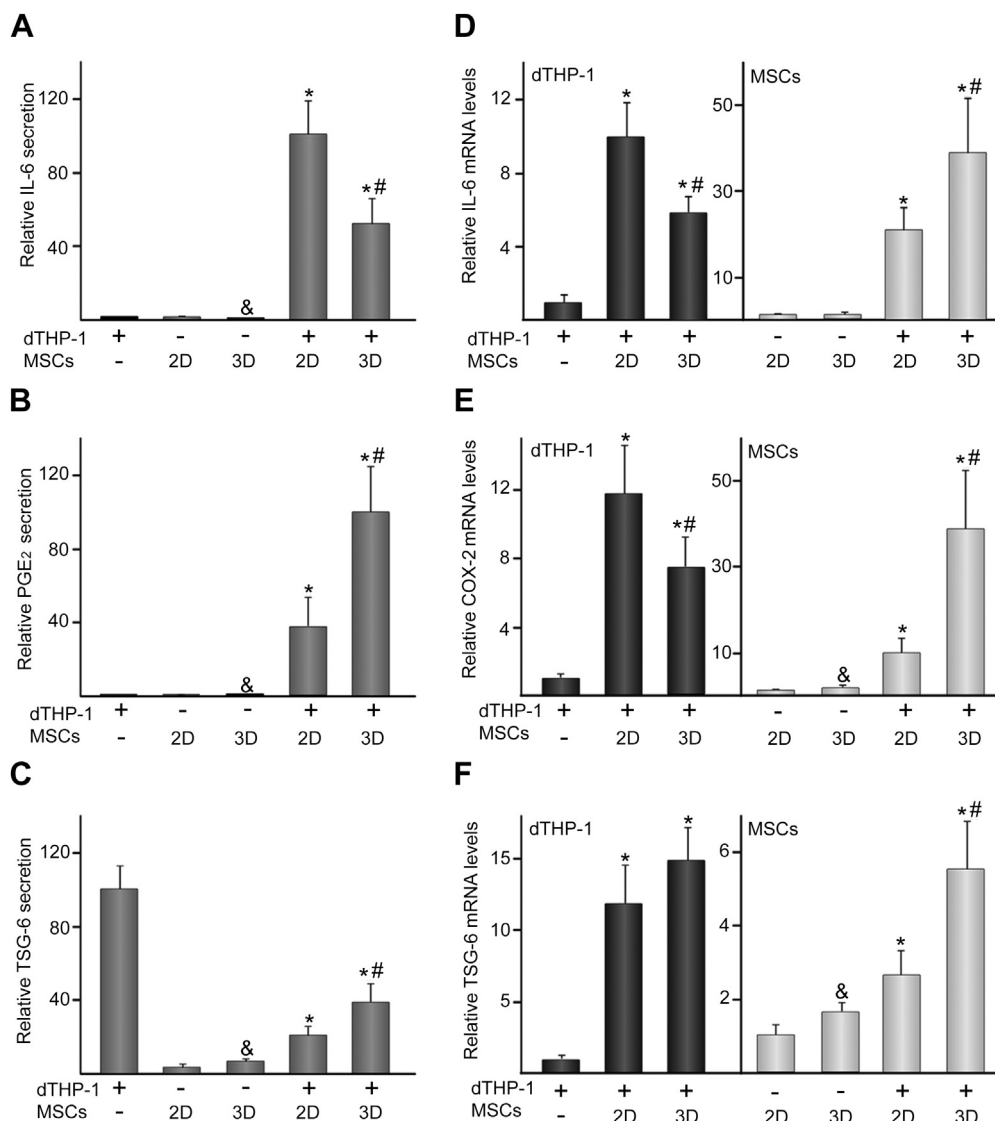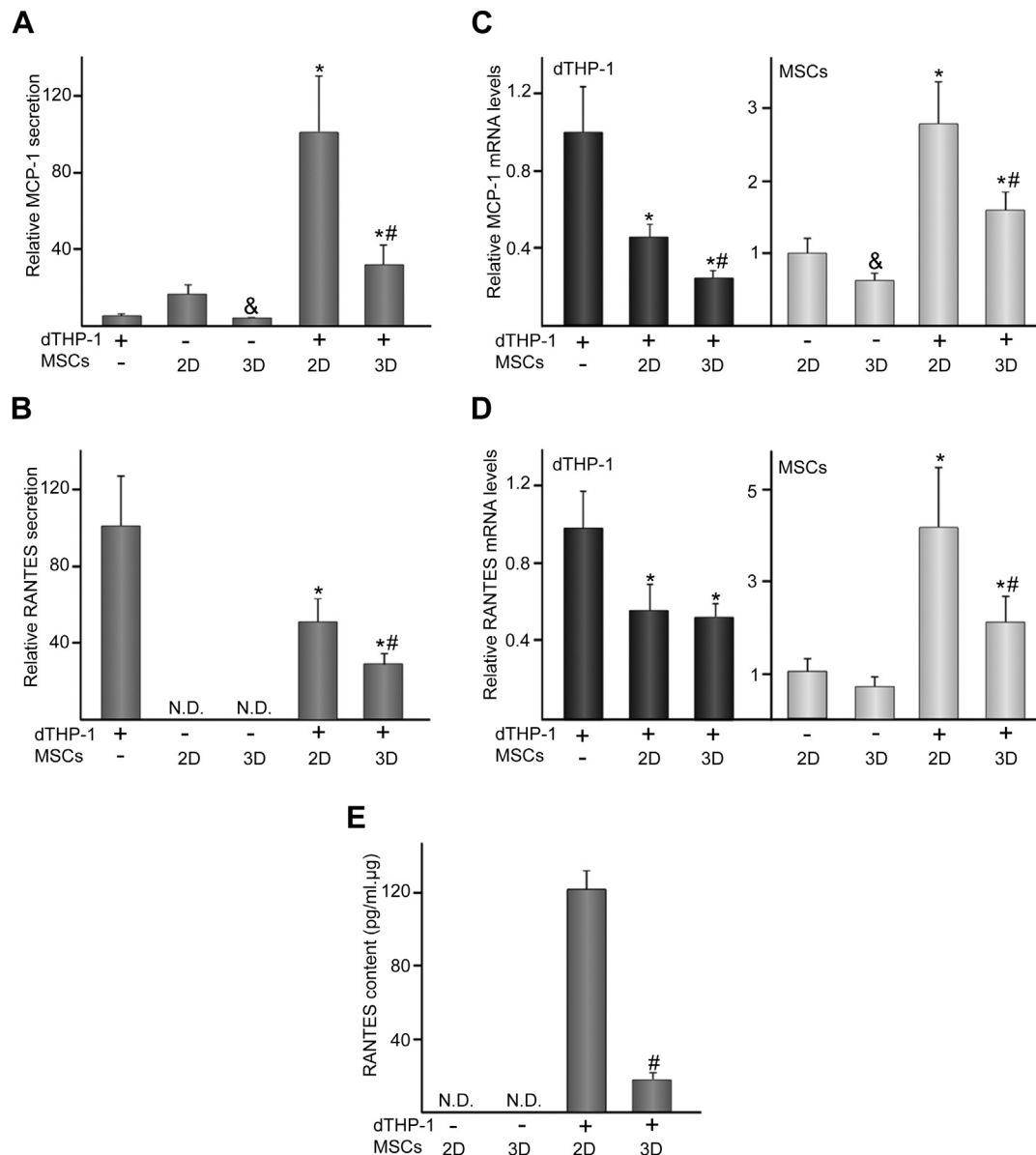


**Fig. 2.** IL-6, PGE₂ and TSG-6 secretion and mRNA levels in 2D or 3D co-cultures. IL-6 (A), PGE₂ (B) and TSG-6 (C) levels in media of dTHP-1, MSCs or dTHP-1/MSC co-cultures. (−) and (+) indicate the absence or presence of the corresponding cell type, where (2D) and (3D) denote MSCs seeded in transwells or scaffolds, respectively. In these experiments, a relative secretion value of 100 corresponded to about 50 ± 9 ng of IL-6, 23 ± 8 ng of PGE₂ and 5 ± 1 ng of TSG-6 per ml of culture medium. *IL-6* (D), *COX-2* (E) and *TSG-6* (F) mRNA levels in dTHP-1 (bars in dark gray) or MSCs (bars in light gray). The data are relative to mRNA levels measured in dTHP-1 or MSCs, which were given the arbitrary value of 1. Each value represents the mean ± SD of seven independent experiments. $^{\&}p < 0.05$ compared to 2D MSCs, $^{*}p < 0.05$ compared to single-cultured cells, $^{\#}p < 0.05$ compared to 2D co-cultures.

or dTHP-1 highly increased after co-culturing (Fig. 2D–F). Interestingly, *IL-6* and *COX-2* expression in co-cultured dTHP-1 decreased when these cells were exposed to 3D MSCs (Fig. 2D, E). In contrast, *IL-6*, *COX-2* and *TSG-6* mRNA levels in 3D co-cultured MSCs were higher than those detected in 2D conditions (Fig. 2D–F).

### 3.5. MCP-1 and RANTES levels in 2D or 3D co-cultures

We explored whether differential arrangements of co-cultured MSCs modulate the release of the chemotactic mediators MCP-1 and RANTES. Compared to single cultures, co-culturing increased MCP-1 secretion but levels were lower in 3D than in 2D settings (Fig. 3A). RANTES was undetectable in cultures of MSCs while dTHP-1 secreted a significant amount of this chemokine (Fig. 3B).

The presence of MSCs in co-cultures reduced RANTES levels, which further decreased in the 3D model. Compared to single-cultured cells, *MCP-1* and *RANTES* mRNA levels decreased in co-cultured dTHP-1 (Fig. 3C, D). *MCP-1* expression in dTHP-1 was further down-regulated by 3D arrangement of MSCs (Fig. 3C). Gene expression quantification of these chemokines in MSCs revealed a significant mRNA accumulation after co-culturing with dTHP-1 (Fig. 3C, D). Interestingly, 3D co-cultured MSCs expressed lower *MCP-1* and *RANTES* mRNA levels than in 2D settings. In order to elucidate whether the decrease in RANTES levels observed in 3D co-cultures could be attributed to the stromal cells, we quantified the amount of this chemokine in MSC layers. RANTES was detectable only after co-culturing and in a lower amount in 3D than in 2D settings (Fig. 3E).



**Fig. 3.** MCP-1 and RANTES secretion and mRNA levels in 2D or 3D co-cultures. MCP-1 (A) and RANTES (B) levels in media of dTHP-1, MSCs or dTHP-1/MSC co-cultures. (−) and (+) indicate the absence or presence of the corresponding cell type, where (2D) and (3D) denote MSCs seeded on transwells or scaffolds, respectively. In these experiments, a relative secretion value of 100 corresponded to about $11 \pm 4$ ng of MCP-1 and $833 \pm 195$ pg of RANTES per ml of culture medium. *MCP-1* (C) and *RANTES* (D) mRNA levels in dTHP-1 (bars in dark gray) or MSCs (bars in light gray). The data are relative to mRNA levels measured in dTHP-1 or MSCs, which were given the arbitrary value of 1. RANTES (E) content in layers of single- or co-cultured MSCs. Each value represents the mean $\pm$ SD of seven independent experiments. $^{\&}p < 0.05$ compared to 2D MSCs, $^{*}p < 0.05$ compared to single-cultured cells, $^{\#}p < 0.05$ compared to 2D co-cultures. N.D.: not detected.

### 3.6. Effect of blocking antibodies on IL-6 and MCP-1 secretion and monocyte migration

To assess whether $PGE_2$ and TSG-6 were involved in the reduction of IL-6 levels in 3D settings, cells were co-cultured in the presence or absence of neutralizing antibodies directed against these mediators. Treatment of co-cultures with anti-$PGE_2$ antibody attenuated IL-6 release, independently of the topographic features of the substrate (Fig. 4A). In contrast, addition of anti-TSG-6 antibody to co-cultures enhanced IL-6 levels in both 2D and 3D settings. Next, we assessed whether IL-6 regulated MCP-1 secretion, and vice versa, in co-cultures (Fig. 4B). Exposure of 2D co-cultures to anti-MCP-1 antibody decreased IL-6 secretion, reaching comparable levels to those detected in 3D conditions. IL-6 production in 3D co-cultures was further attenuated after incubation with anti-MCP-1 antibody. Addition of anti-IL-6 antibody decreased MCP-1
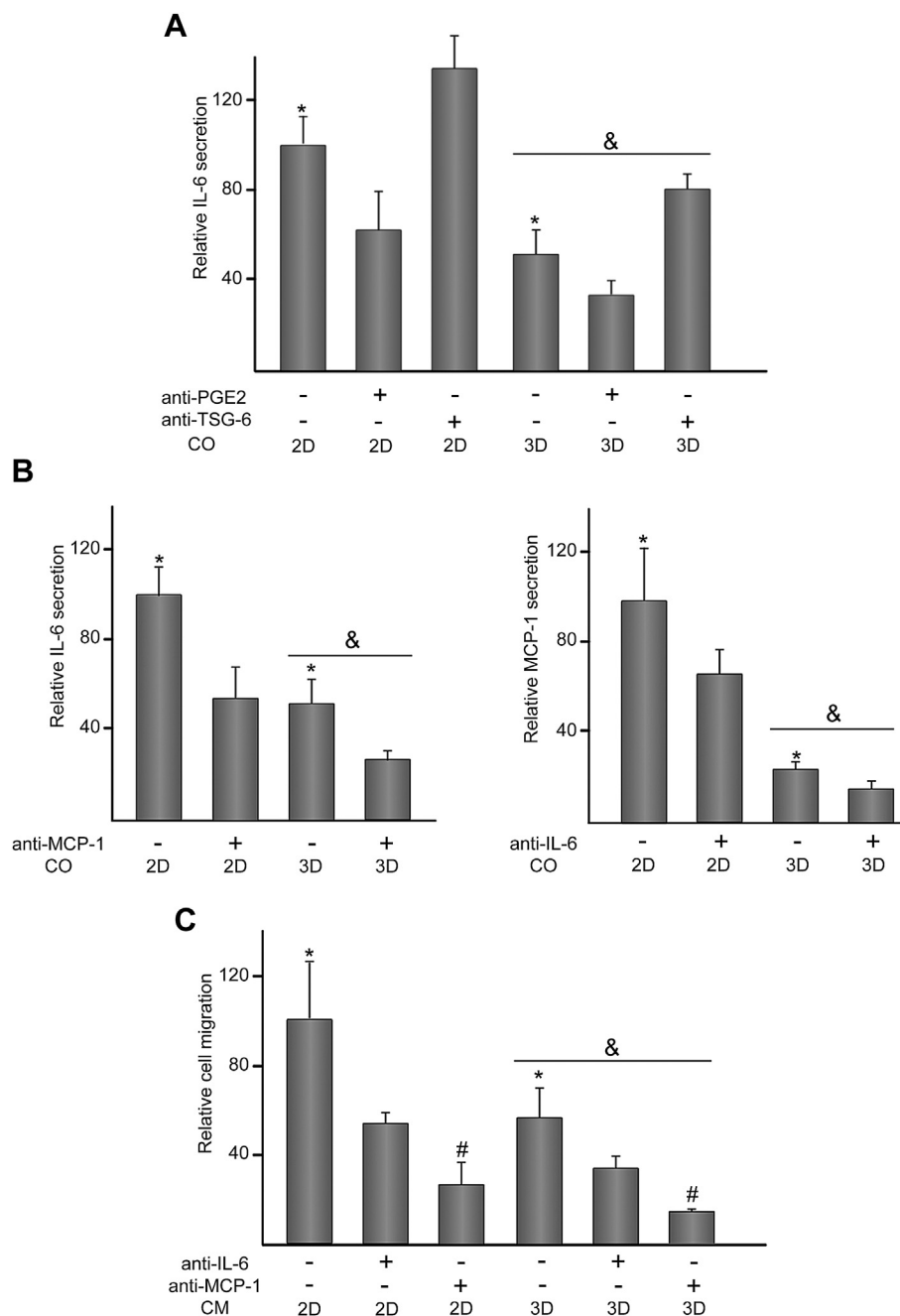


**Fig. 4.** Effect of antibodies treatment on 2D and 3D co-cultures and monocyte migration. (A) IL-6 levels in media of 2D and 3D co-cultures (CO) either untreated (−) or treated (+) with 1 μg/ml anti-$PGE_2$ or anti-TSG-6. In these experiments, a relative secretion value of 100 corresponded to about $34 \pm 5$ ng of IL-6 per ml of culture medium. (B) IL-6 or MCP-1 levels in media of 2D and 3D co-cultures (CO) either untreated (−) or treated (+) with 1 μg/ml anti-MCP-1 or anti-IL-6, respectively. In these experiments, a relative secretion value of 100 corresponded to about $36 \pm 5$ ng of IL-6 and $6 \pm 2$ ng of MCP-1 per ml of culture medium. (C) Migration capacity of THP-1 cells toward conditioned medium (CM) of 2D and 3D co-cultures either untreated (−) or treated (+) with 1 μg/ml anti-IL-6 or anti-MCP-1. In these experiments, a relative value of 100 corresponded to about $56 \pm 15 \times 10^3$ migrated cells. (2D) and (3D) indicate the presence of MSCs seeded on transwells or scaffolds, respectively. Each value represents the mean ± S.D. of six independent experiments. *$p < 0.05$ compared to CO or cells exposed to CM incubated in the presence of antibodies; &$p < 0.05$ compared to 2D settings or CM obtained from 2D settings; #$p < 0.05$ compared to CO or cells exposed to CM incubated in the presence of anti-IL-6 antibody.

production in both 2D and 3D co-cultures. Since IL-6 and MCP-1 display chemotactic activity for monocytes, we studied whether THP-1 migration to CM obtained from 2D and 3D co-cultures was regulated by these chemokines (Fig. 4C). Compared to 2D settings, THP-1 recruitment was reduced when CM of 3D co-cultures was employed as stimulus. THP-1 migration significantly decreased after incubation of CM with anti-IL-6 antibody and even further when anti-MCP-1 was used. The chemotactic activity of CM incubated with anti-IL-6 or anti-MCP-1 antibody was inhibited to a similar degree in 2D or 3D co-cultures.

## 4. Discussion

Increasing evidence suggests that topographical cues play an important role in the determination of MSC functionality. Cells in living tissues are organized into a 3D geometry considerably more complex than dispositions observed in conventional 2D cultures. When embedded in a 3D ECM, MSCs assume a more rounded and polygonal morphology different than that of the unnatural morphology they display in flat substrates [17]. Data herein support that MSCs are sensitive to substrate dimension, exhibiting a stellate morphology and a higher volume/surface area ratio in cellular length scale porous structures than in 2D surfaces. Architectural cues of scaffolds provide not only an appropriate template for structural guidance of MSCs but also a 3D environment that may direct their functional activity. We observed that MSCs cultured in 3D surfaces retain their undifferentiated stage and ability to differentiate into the osteoblastic lineage. While many studies have characterized the effect of scaffold micro-architecture on MSC fate toward osteoblastic differentiation [25,26], little attention has been paid to the influence on MSC immunomodulatory properties. Our results indicate that porous structures activate MSCs to produce $PGE_2$ and TSG-6, postulated as major local anti-inflammatory mediators for these cells [16]. These data are consistent with previous results showing that aggregation of MSCs in 3D spheroids increased the release of both soluble factors [27,28]. In addition, we found that the production of IL-6, MCP-1 and RANKL, immune mediators involved in inflammation and bone resorption, was attenuated in 3D substrates. Therefore, our findings suggest that porous structures drive MSCs into a 3D arrangement that enhance their immune regulatory properties.

While mechanisms underlying the immunomodulatory functions of MSCs on macrophages have been extensively explored [14,15,28,29], there is scarce information about the effect of topographical signals on the regulation of MSC activation and paracrine signaling. Co-culture of spheroid MSCs turned inflammatory macrophages into a regulatory phenotype characterized by reduced secretion of TNF-$\alpha$ [27]. A significant increase in IL-10 secretion, a potent anti-inflammatory mediator, was also observed in cultures of activated macrophages exposed to conditioned medium from spheroid MSCs [28]. In contrast, other authors have reported increased levels of pro-inflammatory cytokines such as IL-1$\beta$, TNF-$\alpha$ and IFN-$\gamma$ in macrophages cultured on hydrogels harboring MSCs [30]. These apparent discrepancies might be explained by the different *in vitro* models employed and reiterate that cell functionality is governed by interactions with the surrounding microenvironment and/or neighboring cells. We found that co-culturing dTHP-1 with MSCs markedly decreased the secretion of TNF-$\alpha$ while conversely stimulated the production of IL-10. The switch of macrophages into IL-10-producing cells has been postulated as a result of the effects of $PGE_2$ and IL-6 secreted by MSCs [31], both highly increased in our co-culture model. Compared to 2D settings, 3D spatial arrangement of co-cultured MSCs highly increases $PGE_2$ secretion and *COX-2* mRNA levels in MSCs. Increased levels of $PGE_2$ in 3D co-cultures correlated well with a reduction in M-CSF and

GM-CSF release, both mediators involved in regulating the cell number and maturation stage of the monocyte/macrophage lineage population [32]. In this regard, $PGE_2$ has been shown to inhibit M-CSF and GM-CSF secretion from fibroblasts or smooth muscle cells stimulated with inflammatory cytokines [33,34]. On the other hand, co-culturing MSCs and dTHP-1 induced a remarkable increase in VEGF production, which in turn may promote endothelial cell proliferation and migration. This effect, however, was not influenced by the topography of the substrate.

IL-6 and TSG-6 have been suggested to be involved in the paracrine anti-inflammatory properties of MSCs [27,35]. Our results show that treatment with anti-$PGE_2$ antibody reduced IL-6 secretion, indicating the $PGE_2$-dependence of IL-6 production in our co-culture model. The increase in $PGE_2$ levels elicited by 3D topography sensing correlated with an increased of *IL-6* mRNA levels in co-cultured MSCs but not with an induction of IL-6 secretion. Further layers of regulation of *IL-6* gene expression or even an increase of IL-6 bound to its soluble receptor may underlie the lower detected levels of the secreted protein. TSG-6 is an inflammation-induced factor that binds to a diverse variety of proteins and glycosaminoglycan ligands, including hyaluronan and fibronectin and is able to modulate NF$\kappa$B-mediated inflammatory signaling pathways [36,37]. Recently, TSG-6 has been identified as a soluble binding protein for the chemotactic and inflammatory cytokine IL-8 [38]. Here, we observe that treatment of co-cultures with anti-TSG-6 increased the levels of IL-6 in media, suggesting that TSG-6 may be mediating its immune regulatory effect through the down-regulation of IL-6 protein synthesis or through its interaction with this cytokine. Interestingly, co-culturing with MSCs strongly decreased the TSG-6 levels detected in single-cultured macrophages. As treatment of macrophages with MSCs-conditioned medium was ineffective to decrease the amount of TSG-6 (data not shown), we hypothesized that this protein might be interacting with fibronectin extracellular matrix synthesized by MSCs, as previously reported in human fibroblasts [36]. TSG-6 has also been postulated as a regulator of bone remodeling through its interaction with RANKL, the primary regulator of osteoclastic differentiation and activation [39]. Supporting this, 3D arrangement of co-cultured MSCs elicited a decrease in RANKL, which correlates with increased levels of TSG-6. The low concentration of RANKL in the co-culture media and the short exposure period of macrophages to it are not enough to drive these cells towards osteoclast lineage [40]. However, topographical features of the substrate may modulate the interactions that MSCs establish with macrophages after *in vivo* implantation to regulate osteoclast generation or activity.

Another relevant aspect of our study was that MCP-1 and RANTES are susceptible to modulation by differentially arranged MSCs, as secreted levels of both proteins were substantially lower in 3D than in 2D co-cultures. These chemotactic factors have been related to the infiltration or trafficking of peripheral blood monocytes, modulating cellular recruitment to the implant site [2]. Large numbers of monocyte-derived macrophages are generally associated with the formation of a granulation tissue, which interferes with the implant integration within the host [8]. Compared to single-cultured cells, *MCP-1* mRNA levels increased in co-cultured MSCs while diminished in macrophages, suggesting that stromal cells are the main contributors to the overall secreted levels. Interestingly, secretion of MCP-1 was lower in 3D than in 2D co-cultures, an effect that paralleled gene expression pattern in MSCs. Secreted RANTES was significantly lower after co-culturing macrophages with MSCs, an effect regulated at the mRNA level. This protein was undetectable in cell layers or media of single cultures of MSCs, but clearly detectable in co-cultures. 3D spatial arrangement of co-cultured MSCs diminished RANTES secretion

and caused a strong reduction in its intracellular protein and mRNA levels. This suggests that the regulation of this cytokine in the co-cultures is mainly mediated by stromal cells and can be modulated by the micro-architecture of the substrate.

It is noteworthy that secretion pattern of MCP-1 in co-cultures closely resembled that of IL-6, which also may act as a classical chemokine for monocytic lineage cells [7]. Positive regulation between IL-6 and MCP-1 has been addressed in myeloma and tubular epithelial cells [41,42]. Our study using neutralizing antibodies revealed that MCP-1 production in co-cultures was positively regulated by IL-6. Also, IL-6 levels decreased in response to anti-MCP-1 antibody treatment, suggesting that both chemotactic cytokines up-regulate each other's secretion. As expected, conditioned medium of 3D co-cultures decreased monocyte migration and this effect was mediated, at least in part, by reduced levels of IL-6 and MCP-1. Control of cellular recruitment or trafficking to the injury site by 3D arrangement of MSCs could be exploited as an efficient strategy to ameliorate excessive inflammatory response after material implantation. Moreover, since osteoclasts are derived from hematopoietic progenitors in the monocyte/macrophage lineage, we hypothesized that reduction in monocyte migration induced by microporous cues might contribute to bone regeneration.

Fig. 5 summarizes the main findings of this work. 3D topography sensing activates MSCs to produce $PGE_2$ and TSG-6 anti-inflammatory proteins while attenuates the release of IL-6, MCP-1, RANTES, GM-CSF, M-CSF and RANKL in co-cultures with macrophages. Compared to 2D co-cultures, local inflammatory milieu provided by 3D-arranged MSCs reduces monocyte migration and this effect was mediated, at least in part, by reduced levels of IL-6 and MCP-1. This study shows a substrate-dependent paracrine signaling between MSCs and macrophages

and highlights the importance of 3D substrate geometry in the soluble factor-guided communication. Progress in fabrication technologies of tissue-engineering scaffolds allows researchers to create substrates mimicking characteristics of the _in vivo_ physiological topography. Further exploration of the influence of topographical cues on MSC immunomodulatory properties will lead to a more complete understanding of the mechanism of MSC-mediated tissue repair and will provide the framework for manufacturing bio-inspired scaffolds for novel tissue-engineering approaches.

## 5. Conclusions

We investigated the effect of topographical cues of scaffolds on paracrine interactions that MSCs establish with macrophages. MSCs cultured in 3D substrates retain their undifferentiated stage and ability to differentiate into the osteoblastic lineage. Microporous features of the culture substrate drive MSCs into a spatial arrangement that stimulates the production of the anti-inflammatory proteins $PGE_2$ and TSG-6. Compared to 2D settings, 3D arrangement of MSCs co-cultured with macrophages significantly attenuates the secretion of IL-6 and MCP-1. The interplay between $PGE_2$, IL-6, TSG-6 and MCP-1 in co-cultures is markedly influenced by the 3D geometry of the substrate. Compared to 2D monolayer cells, local inflammatory milieu provided by 3D-arranged MSCs in co-cultures induces a decrease in monocyte migration. This effect is attributed, at least in part, to a reduction in the production of IL-6 and MCP-1, proteins that up-regulate each other's secretion. Our results reveal that interactions between MSCs and macrophages through soluble factors are strongly dependent on the micro-architecture that supports the stromal cells.
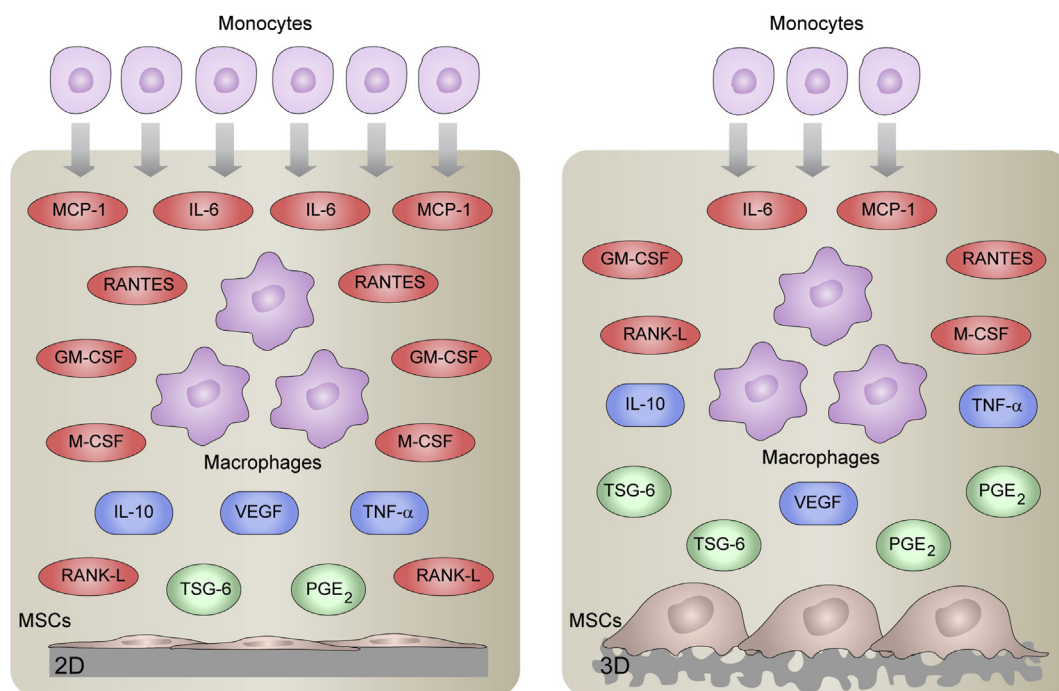


**Fig. 5.** Overview of the effect of topographical cues in the soluble factor-guided communication between MSCs and macrophages. MSCs were seeded in 2D substrates (left panel) or 3D scaffolds (right panel) and co-cultured with macrophages using a transwell insert system. The figure illustrates soluble factors whose levels decreased (red), increased (green) or were not affected (blue) in 3D co-cultures as compared to 2D settings. 3D topography sensing activates MSCs to produce $PGE_2$ and TSG-6 anti-inflammatory proteins while attenuates the secretion of IL-6, MCP-1, RANTES, GM-CSF, M-CSF and RANKL in co-cultures with macrophages. TNF-α, IL-10 and VEGF levels are unaffected by topographical features of the substrate. The lower number of monocytes in 3D settings represents the decrease in monocyte migration to the local inflammatory milieu provided by 3D-arranged MSCs as compared to 2D co-cultures. This attenuation in monocyte recruitment is mediated, at least in part, by reduced levels of IL-6 and MCP-1 (For interpretation of the references to color in this figure legend, the reader is referred to the web version of this article.).

## Acknowledgments

## References

[1] Mallick KK, Cox SC. Biomaterial scaffolds for tissue engineering. Front Biosci 2013;5:341–60.

[2] Anderson JM, Rodriguez A, Chang DT. Foreign body reaction to biomaterials. Semin Immunol 2008;20:86–100.

[3] Bryers JD, Giachelli CM, Ratner BD. Engineering biomaterials to integrate and heal: the biocompatibility paradigm shifts. Biotechnol Bioeng 2012;109: 1898–911.

[4] Bridges AW, Whitmire RE, Singh N, Templeman KL, Babensee JE, Lyon LA, et al. Chronic inflammatory responses to microgel-based implant coatings. J Biomed Mater Res A 2010;94:252–8.

[5] Ehashi T, Takemura T, Hanagata N, Minowa T, Kobayashi H, Ishihara K, et al. Comprehensive genetic analysis of early host body reactions to the bioactive and bio-inert porous scaffolds. PLoS One 2014;9:e85132.

[6] Eming SA, Krieg T, Davidson JM. Inflammation in wound repair: molecular and cellular mechanisms. J Invest Dermatol 2007;127:514–25.

[7] Clahsen T, Schaper F. Interleukin-6 acts in the fashion of a classical chemokine on monocytic cells by inducing integrin activation, cell adhesion, actin polymerization, chemotaxis, and transmigration. J Leukoc Biol 2008;84:1521–9.

[8] Brown BN, Ratner BD, Goodman SB, Amar S, Badylak SF. Macrophage polarization: an opportunity for improved outcomes in biomaterials and regenerative medicine. Biomaterials 2012;33:3792–802.

[9] Mastri M, Lin H, Lee T. Enhancing the efficacy of mesenchymal stem cell therapy. World J Stem Cells 2014;6:82–93.

[10] Bassi EJ, De Almeida DC, Moraes-Vieira PM, Câmara NO. Exploring the role of soluble factors associated with immune regulatory properties of mesenchymal stem cells. Stem Cell Rev 2012;8:329–42.

[11] Ma S, Xie N, Li W, Yuan B, Shi Y, Wang Y. Immunobiology of mesenchymal stem cells. Cell Death Differ 2014;21:216–25.

[12] Mountziaris PM, Mikos AG. Modulation of the inflammatory response for enhanced bone tissue regeneration. Tissue Eng Part B Rev 2008;14:179–86.

[13] Eggenhofer E, Hoogduijn MJ. Mesenchymal stem cell-educated macrophages. Transplant Res 2012;12:1–5.

[14] Kim J, Hematti P. Mesenchymal stem cell-educated macrophages: a novel type of alternatively activated macrophages. Exp Hematol 2009;37:1445–53.

[15] Maggini J, Mirkin G, Bognanni I, Holmberg J, Piazzon IM, Nepomnaschy I, et al. Mouse bone marrow-derived mesenchymal stromal cells turn activated macrophages into a regulatory-like profile. PLoS One 2010;5:e9252.

[16] English K. Mechanisms of mesenchymal stromal cell immunomodulation. Immunol Cell Biol 2013;91:19–26.

[17] Baker BM, Chen CS. Deconstructing the third dimension: how 3D culture microenvironments alter cellular cues. J Cell Sci 2012;125:3015–24.

[18] Wang L, Carrier R. Biomimetic topography: bioinspired cell culture substrates and scaffolds. In: Cavrak M, editor. Advances in Biomimetics. InTech; 2011. p. 453–72.

[19] Rodriguez-Lorenzo LM, Saldaña L, Benito-Garzón L, García-Carrodeguas R, de Aza S, Vilaboa N, et al. Feasibility of ceramic-polymer composite cryogels as scaffolds for bone tissue engineering. J Tissue Eng Regen Med 2012;6:421–33.

[20] Wei J, Han J, Zhao Y, Cui Y, Wang B, Xiao Z, et al. The importance of three-dimensional scaffold structure on stemness maintenance of mouse embryonic stem cells. Biomaterials 2014;35:7724–33.

[21] Wang M, Cheng X, Zhu W, Holmes B, Keidar M, Zhang LG. Design of biomimetic and bioactive cold plasma-modified nanostructured scaffolds for enhanced osteogenic differentiation of bone marrow-derived mesenchymal stem cells. Tissue Eng Part A 2014;20:1060–71.

[22] Knight E, Murray B, Carnachan R, Przyborski S. Alvetex®: polystyrene scaffold technology for routine three dimensional cell culture. Methods Mol Biol 2011;695:323–40.

[23] Saldaña L, Crespo L, Bensiamar F, Arruebo M, Vilaboa N. Mechanical forces regulate stem cell response to surface topography. J Biomed Mater Res A 2014;102:128–40.

[24] Vallés G, Gil-Garay E, Munuera L, Vilaboa N. Modulation of the cross-talk between macrophages and osteoblasts by titanium-based particles. Biomaterials 2008;29:2326–35.

[25] Kim K, Dean D, Wallace J, Breithaupt R, Mikos AG, Fisher JP. The influence of stereolithographic scaffold architecture and composition on osteogenic signal expression with rat bone marrow stromal cells. Biomaterials 2011;32: 3750–63.

[26] Phadke A, Hwang Y, Kim SH, Kim SH, Yamaguchi T, Masuda K, et al. Effect of scaffold microarchitecture on osteogenic differentiation of human mesenchymal stem cells. Eur Cell Mater 2013;25:114–28.

[27] Bartosh TJ, Ylöstalo JH, Mohammadipoor A, Bazhanov N, Coble K, Claypool K, et al. Aggregation of human mesenchymal stromal cells (MSCs) into 3D spheroids enhances their antiinflammatory properties. Proc Natl Acad Sci U S A 2010;107:13724–9.

[28] Ylöstalo JH, Bartosh TJ, Coble K, Prockop DJ. Human mesenchymal stem/stromal cells cultured as spheroids are self-activated to produce prostaglandin E$_2$ that directs stimulated macrophages into an anti-inflammatory phenotype. Stem Cells 2012;30:2283–96.

[29] Anton K, Banerjee D, Glod J. Macrophage-associated mesenchymal stem cells assume an activated, migratory, pro-inflammatory phenotype with increased IL-6 and CXCL10 secretion. PLoS One 2012;7:e35036.

[30] King SN, Hanson SE, Chen X, Kim J, Hematti P, Thibeault SL. In vitro characterization of macrophage interaction with mesenchymal stromal cell-hyaluronan hydrogel constructs. J Biomed Mater Res A 2014;102:890–902.

[31] Bernardo ME, Fibbe WE. Mesenchymal stromal cells: sensors and switchers of inflammation. Cell Stem Cell 2013;13:392–402.

[32] Moss ST, Hamilton JA. Proliferation of a subpopulation of human peripheral blood monocytes in the presence of colony stimulating factors may contribute to the inflammatory process in diseases such as rheumatoid arthritis. Immunobiology 2000;202:18–25.

[33] Agro A, Langdon C, Smith F, Richards CD. Prostaglandin E$_2$ enhances interleukin 8 (IL-8) but inhibits GMCSF production by IL-1 stimulated human synovial fibroblasts in vitro. J Rheumatol 1996;23:862–8.

[34] Inoue H, Takamori M, Shimoyama Y, Ishibashi H, Yamamoto S, Koshihara Y. Regulation by PGE$_2$ of the production of interleukin-6, macrophage colony stimulating factor, and vascular endothelial growth factor in human synovial fibroblasts. Br J Pharmacol 2002;136:287–95.

[35] Bouffi C, Bony C, Courties G, Jorgensen C, Noël D. IL-6-dependent PGE$_2$ secretion by mesenchymal stem cells inhibits local inflammation in experimental arthritis. PLoS One 2010;5:e14247.

[36] Kuznetsova SA, Mahoney DJ, Martin-Manso G, Ali T, Nentwich HA, Sipes JM, et al. TSG-6 binds via its CUB_C domain to the cell-binding domain of fibronectin and increases fibronectin matrix assembly. Matrix Biol 2008;27: 201–10.

[37] Prockop DJ, Oh JY. Mesenchymal stem/stromal cells (MSCs): role as guardians of inflammation. Mol Ther 2012;20:14–20.

[38] Dyer DP, Thomson JM, Hermant A, Jowitt TA, Handel TM, Proudfoot AE, et al. TSG-6 inhibits neutrophil migration via direct interaction with the chemokine CXCL8. J Immunol 2014;192:2177–85.

[39] Mahoney DJ, Mikecz K, Ali T, Mabilleau G, Benayahu D, Plaas A, et al. TSG-6 regulates bone remodeling through inhibition of osteoblastogenesis and osteoclast activation. J Biol Chem 2008;283:25952–62.

[40] Sengupta S, Park SH, Seok GE, Patel A, Numata K, Lu CL, et al. Quantifying osteogenic cell degradation of silk biomaterials. Biomacromolecules 2010;11: 3592–9.

[41] Arendt BK, Velazquez-Dones A, Tschumper RC, Howell KG, Ansell SM, Witzig TE, et al. Interleukin 6 induces monocyte chemoattractant protein-1 expression in myeloma cells. Leukemia 2002;16:2142–7.

[42] Viedt C, Dechend R, Fei J, Hänsch GM, Kreuzer J, Orth SR. MCP-1 induces inflammatory activation of human tubular epithelial cells: involvement of the transcription factors, nuclear factor-kappaB and activating protein-1. J Am Soc Nephrol 2002;13:1534–47.